

Bandwidth Selection for Spatial HAC Standard Errors

Alexander Lehner*

2026-03-03

Spatial autocorrelation in regression models can lead to downward biased standard errors and thus incorrect inference. The most common correction in applied economics is the spatial heteroskedasticity and autocorrelation consistent (HAC) standard error estimator introduced by Conley (1999). A critical input is the kernel bandwidth: the distance within which residuals are allowed to be correlated. However, this is still an unresolved problem and there is no formal guidance in the literature. In this paper, I first document that the relationship between the bandwidth and the magnitude of spatial HAC standard errors is inverse-U shaped. This implies that both too narrow and too wide bandwidths lead to underestimated standard errors, contradicting the conventional wisdom that wider bandwidths yield more conservative inference. I then propose a simple, non-parametric, data-driven bandwidth selector based on the empirical covariogram of regression residuals. In extensive Monte Carlo experiments calibrated to empirically relevant spatial correlation structures across the contiguous United States, I show that the proposed method controls the false positive rate at or near the nominal 5% level across a wide range of spatial correlation intensities and sample configurations. I compare six kernel functions and find that the Bartlett and Epanechnikov kernels deliver the best size control. An empirical application using U.S. county-level data illustrates the practical relevance of the method. The R package `SpatialInference` implements the proposed bandwidth selection method.

Keywords: Spatial autocorrelation, Conley standard errors, HAC inference, bandwidth selection, covariogram, kernel estimation, Monte Carlo simulation

JEL Classification: C14, C21, C52

*World Bank Group, Outcomes Department, 1818 H Street, Washington, DC. Email: alehner@worldbank.org. I thank audiences at UChicago for helpful comments and discussions. Alex Gordon provided excellent research assistance. Computations were carried out on the Akropolis cluster at the University of Chicago. The findings, interpretations, and conclusions expressed in this paper are entirely those of the author and do not necessarily represent the views of the World Bank Group, its Executive Directors, or the countries they represent.

1 Introduction

The concept of spatial autocorrelation has served as an organizing principle in spatial statistics for many decades, dating back at least to [Student \[1914\]](#)’s article on “the elimination of spurious correlation due to position in time and space.” [Student \[1914\]](#) demonstrated that the application of conventional statistical methods to autocorrelated observations “would lead to altogether misleading values” (p. 179) and presented adjusted inferences as evidence of the importance of such corrections. In the modern econometrics literature, the problems for statistical inference induced by spatial autocorrelation have been recognized since at least [Anselin and Griffith \[1988\]](#), who showed that spatial effects can substantially distort regression-based inference. Given that virtually all economic data have spatial structure—and that georeferenced data are becoming ubiquitous—this is a growing concern in applied research. The importance of accounting for dependence in inference has been highlighted in many contexts: [Bertrand et al. \[2004\]](#) demonstrated the severity of the problem in panel data with temporal correlation, and casual empiricism suggests that applied researchers are now acutely aware of the potential for distortions. Yet for spatial correlation, no equivalent practical guidance on how to operationalize the correction has emerged.

The most common approach to address spatial autocorrelation in regression analysis in economics and many other social sciences is to rely on spatial heteroskedasticity and autocorrelation consistent (HAC) standard errors, introduced in the seminal contribution of [Conley \[1999\]](#). Conley extended the logic of [Newey and West \[1987\]](#) from time-series to the two-dimensional spatial domain, building on the HAC framework of [Andrews \[1991\]](#). The core of the technique is a non-parametric estimator for the variance-covariance matrix that uses kernel-weighted averages of cross-products of residuals, where the kernel downweights pairs of observations as a function of the distance between them. A key input for operationalizing this estimator is the choice of a *cutoff bandwidth*—the distance beyond which residuals are assumed to be uncorrelated. In the time-series analogue, a rich literature on automated and rule-of-thumb bandwidth selection exists [e.g., [Newey and West, 1987](#), [Andrews, 1991](#), [Sun, 2014](#)]. For the spatial case, however, no widely adopted equivalent exists. Instead, researchers typically rely on ad hoc choices guided by intuition or domain knowledge, creating what [Gelman and Loken \[2013\]](#) term “researcher degrees of freedom.”

This paper makes three contributions. First, I document an empirical regularity with important implications for spatial HAC estimation: the relationship between the bandwidth and the magnitude

of spatial HAC standard errors follows an *inverse-U shape*. This means that both too narrow and too wide bandwidths lead to underestimated standard errors and thus to overrejection of true null hypotheses. This finding contradicts the prevailing conventional wisdom in applied work, which holds that choosing wider bandwidths ensures conservative inference.

Second, I propose a simple, non-parametric, data-driven method to select the appropriate bandwidth. The method is based on the empirical covariogram of regression residuals: the estimated bandwidth corresponds to the distance at which residual covariation first crosses zero. Third, I conduct extensive Monte Carlo simulations to evaluate the method. Using spatial correlation structures calibrated to the geography of the contiguous United States, I show that the proposed bandwidth selector controls the false positive rate at or near the nominal 5% level across a wide range of spatial autocorrelation intensities, sample sizes, and spatial configurations. The simulations also provide a systematic comparison of six commonly used kernel functions—Bartlett, Uniform, Epanechnikov, Gaussian, Parzen, and Quartic Biweight—for spatial HAC estimation, finding that the Bartlett and Epanechnikov kernels deliver the best size control.

Related literature. The most closely related work is [Kim and Sun \[2011\]](#), who derive the MSE-optimal bandwidth for spatial HAC estimation and propose a parametric plug-in estimator. Their optimal bandwidth is a function of the sample size (n^α for some $\alpha > 0$), which contrasts with the approach proposed here. The plug-in estimator of [Kim and Sun \[2011\]](#) relies on parametric pilot estimators of unknown quantities, whereas the covariogram-range method proposed in this paper is fully non-parametric and does not require such assumptions. [Kelejian and Prucha \[2007\]](#) provide a detailed treatment of the spatial HAC estimator’s properties and derive consistency results; the present paper builds on their theoretical framework.

Recent contributions have taken a different approach by proposing inference methods that bypass the Conley HAC framework altogether. [Müller and Watson \[2022\]](#) and [Müller and Watson \[2023\]](#) develop spatial correlation principal components (SCPC) confidence intervals that are robust to arbitrary spatial correlation without requiring bandwidth selection. [Müller and Watson \[2024\]](#) show that spatial I(1) processes can induce spuriously significant regression results even with spatial HAC or cluster-robust standard errors, and propose spatial differencing methods. [Conley and Kelly \[2025\]](#) propose spatial basis regressions combined with placebo tests for persistence studies. [DellaVigna et al. \[2025\]](#) use multiple outcome variables to estimate cross-sectional dependence, sidestepping the bandwidth problem entirely. While each of these methods has merit, they also

require departures from the familiar regression framework that applied researchers are accustomed to. The present paper demonstrates that valid inference can be achieved *within* the standard Conley HAC framework—provided the bandwidth is chosen appropriately. The method is transparent, intuitive, and computationally efficient.

In the time-series HAC literature, [Kolokotronis et al. \[2024\]](#) show that the Bartlett (Newey–West) kernel delivers the highest power among first-order kernels. The present paper extends the comparison of kernel functions to the spatial domain, where such a systematic evaluation has not been conducted.

The rest of the paper is organized as follows. Section 2 introduces the econometric framework and the spatial HAC estimator. Section 3 presents the proposed bandwidth selection method with formal assumptions and a consistency result. Section 4 describes the simulation design for generating spatially correlated data. Section 5 documents the inverse-U relationship. Section 7 presents the Monte Carlo results. Section 8 provides an empirical application. Section 9 concludes. Section 11 contains additional details on spatial HAC estimation, kernel functions, and the geostatistical simulation procedure.

2 Econometric Framework

2.1 The Linear Model with Spatially Correlated Errors

Let $\mathcal{S} \subset \mathbb{R}^2$ be a subset of two-dimensional Euclidean space and let $\mathbf{s}_i = (s_{1i}, s_{2i})' \in \mathcal{S}$ denote the spatial location of observation i , with s_{1i} and s_{2i} representing the two spatial coordinates.¹ Consider the linear regression model

$$y_i = \mathbf{x}_i' \beta + \varepsilon_i, \quad i = 1, \dots, n, \quad (1)$$

where $y_i \equiv y(\mathbf{s}_i)$ is the outcome at location \mathbf{s}_i , \mathbf{x}_i is a $p \times 1$ vector of regressors, β is the parameter vector of interest, and $\varepsilon_i \equiv \varepsilon(\mathbf{s}_i)$ is the error term with $E[\varepsilon_i] = 0$. The error terms fail to satisfy the independence assumption: $\text{Cov}(\varepsilon_i, \varepsilon_j) \neq 0$ for nearby locations \mathbf{s}_i and \mathbf{s}_j . Intuitively, this arises

¹For unprojected geographic data, these correspond to longitude and latitude on the sphere \mathbb{S}^2 . For projected data, they are coordinates in a planar coordinate system. Without loss of generality, this paper refers to locations in \mathbb{R}^2 and implicitly assumes projected data.

because outcomes are not randomly distributed across space; near things tend to be more related than distant things.²

Since the law of large numbers applies to weakly dependent spatial data, the OLS estimator $\hat{\beta}$ remains consistent. The concern when dealing with spatial autocorrelation is therefore *inference*: the standard heteroskedasticity-robust variance estimator

$$\hat{V}_{\text{HC}} = \left(\sum_{i=1}^n \mathbf{x}_i \mathbf{x}'_i \right)^{-1} \left(\sum_{i=1}^n \hat{\varepsilon}_i^2 \mathbf{x}_i \mathbf{x}'_i \right) \left(\sum_{i=1}^n \mathbf{x}_i \mathbf{x}'_i \right)^{-1}$$

ignores cross-products $\hat{\varepsilon}_i \hat{\varepsilon}_j$ for $i \neq j$ and thus underestimates the true variance of $\hat{\beta}$ in the presence of positive spatial autocorrelation. This leads to inflated t -statistics and rejection rates that exceed the nominal level.

2.2 The Spatial HAC Estimator

Conley [1999] proposes a non-parametric estimator for the variance-covariance matrix that accounts for spatial correlation. The spatial HAC estimator takes the form

$$\hat{V}_{\text{SHAC}} = (\mathbf{X}'\mathbf{X})^{-1} \hat{\wedge} (\mathbf{X}'\mathbf{X})^{-1}, \quad (2)$$

where

$$\hat{\wedge} = \sum_{i=1}^n \sum_{j=1}^n K\left(\frac{d_{ij}}{\varsigma}\right) \hat{\varepsilon}_i \hat{\varepsilon}_j \mathbf{x}_i \mathbf{x}'_j. \quad (3)$$

Here, $d_{ij} = d(\mathbf{s}_i, \mathbf{s}_j)$ is the distance between observations i and j , $\varsigma > 0$ is the bandwidth (cutoff distance), and $K(\cdot)$ is a kernel function satisfying $K(0) = 1$, $K(u) = 0$ for $|u| > 1$, and $K(u) = K(-u)$. The kernel downweights the contribution of cross-products as a function of distance, assigning zero weight to pairs separated by more than ς . When $\varsigma = 0$, the estimator reduces to the standard heteroskedasticity-consistent (HC) estimator.

The choice of bandwidth ς is the central concern of this paper. It determines the distance within which residuals are allowed to be correlated and thus directly affects the magnitude of the estimated standard errors.

²This paraphrases Tobler's [1970] first law of geography.

2.3 Kernel Functions

Six kernel functions are considered in this study:

$$\begin{aligned}
 \text{Uniform:} & \quad K(u) = \mathbf{1}(0 \leq u \leq 1) \\
 \text{Bartlett:} & \quad K(u) = (1 - u) \cdot \mathbf{1}(0 \leq u \leq 1) \\
 \text{Epanechnikov:} & \quad K(u) = (1 - u^2) \cdot \mathbf{1}(0 \leq u \leq 1) \\
 \text{Parzen:} & \quad K(u) = \begin{cases} 1 - 6u^2 + 6u^3 & 0 \leq u < 1/2 \\ 2(1 - u)^3 & 1/2 \leq u \leq 1 \end{cases} \\
 \text{Quartic Biweight:} & \quad K(u) = (1 - u^2)^2 \cdot \mathbf{1}(0 \leq u \leq 1) \\
 \text{Gaussian:} & \quad K(u) = \exp(-u^2/2) \cdot \mathbf{1}(0 < u < 1)
 \end{aligned}$$

where $u = d_{ij}/\varsigma$ is the normalized distance. The Uniform kernel assigns equal weight to all pairs within the bandwidth, while the others assign declining weights. The Bartlett kernel corresponds to the spatial analogue of the [Newey and West \[1987\]](#) estimator. The Gaussian kernel used here is truncated at the bandwidth, differing from the standard Gaussian density by omitting the normalization constant; this ensures $K(0) = 1$ and $K(u) = 0$ for $u > 1$, consistent with the spatial HAC framework.

2.4 Measuring Spatial Autocorrelation

In practice, the spatial relations described above are typically accounted for by a connectivity matrix, often referred to as a weighting matrix—a concept dating back to at least [Moran \[1948\]](#). Let \mathbf{W} be the $n \times n$ matrix describing a relationship between all locations $\mathbf{s}_1, \dots, \mathbf{s}_n$, where the (i, j) -th element, $w_{ij} \equiv [\mathbf{W}]_{ij}$, refers to the distance between units i and j . In general, this distance does not have to be spatial but can also refer to, e.g., economic or social distance. If $w_{ij} \neq 0$, units i and j are neighbors. In practice, \mathbf{W} will be a sparse matrix in most empirical applications, meaning that most pairs i and j are not classified as neighbors, i.e., $w_{ij} = 0$.

To illustrate how a spatially lagged variable is constructed, consider the i -th row of the connectivity matrix and x_i , the value of the scalar variable \mathbf{x} for unit i . The spatial lag of x_i can then be written

as

$$[\mathbf{W}\mathbf{x}]_i = w_{i1}x_1 + w_{i2}x_2 + \cdots + w_{in}x_n = \sum_{j=1}^n w_{ij}x_j,$$

which is a weighted sum of the values of the same variable across all neighbors. In practice, the entries of \mathbf{W} are usually row-normalized such that $\sum_{j=1}^n w_{ij} = 1$ for all rows i . Note also that the main diagonal is set to zero, $w_{ii} = 0$, meaning that a unit is not its own neighbor. Put differently, \mathbf{W} can be viewed as the spatial lag operator when operationalized via the matrix product $\mathbf{W}\mathbf{x}$.

To test each regression specification for residual autocorrelation, I rely on Moran's I [Moran, 1950].

In its basic form it can be written as

$$I = \frac{n}{\sum_i \sum_j w_{ij}} \cdot \frac{\sum_{i=1}^n \sum_{j=1}^n w_{ij} (\hat{\varepsilon}_i - \bar{\hat{\varepsilon}})(\hat{\varepsilon}_j - \bar{\hat{\varepsilon}})}{\sum_{i=1}^n (\hat{\varepsilon}_i - \bar{\hat{\varepsilon}})^2},$$

where n is the number of units and $\sum_i \sum_j w_{ij}$ is the sum of all spatial weights. The denominator $\sum_{i=1}^n (\hat{\varepsilon}_i - \bar{\hat{\varepsilon}})^2$ is the variance and the numerator involves the spatial lags discussed above. Note the striking resemblance with Pearson's correlation coefficient: Moran's I quantifies the degree of correlation of $\hat{\varepsilon}_i$ with its spatially lagged neighbors. The expected value under spatial randomness is $E[I] = -1/(n - 1)$ and inference is based on the standardized statistic $Z = (I - E[I])/\sqrt{\text{Var}(I)}$. When applied to regression residuals, the computation accounts for the linear projection following Anselin [1988] and Cliff and Ord [1981]. All Moran's I tests are conducted using the `spdep` package [Bivand et al., 2020].

A drawback when working with connectivity matrices is that they usually have to be defined ex-ante by the researcher. For the present study, this is less of a concern because the matrix is used only for testing, not for estimation. The weights matrix is held constant across all simulations—based on a distance band of 200 km—so that reported Moran's I values are comparable across scenarios. In practice, there are many ways to define a connectivity matrix; this study relies on distance band and k -nearest neighbor specifications.

3 The Covariogram Range Method

3.1 The Empirical Covariogram

The key to the proposed bandwidth selection method is the *empirical covariogram* of regression residuals. For a set of estimated residuals $\hat{\varepsilon}_i$, $i = 1, \dots, n$, the empirical covariogram at lag distance h is

$$\hat{C}(h) = \frac{1}{|N(h)|} \sum_{(i,j) \in N(h)} \hat{\varepsilon}_i \hat{\varepsilon}_j, \quad (4)$$

where $N(h) = \{(i, j) : h - \delta \leq d(\mathbf{s}_i, \mathbf{s}_j) < h + \delta\}$ is the set of all location pairs separated by a distance falling in the bin centered at h with half-width δ , and $|N(h)|$ is the cardinality of this set. The bin width 2δ must be chosen large enough to ensure sufficient observations per bin. In practice, this amounts to specifying a number of equally spaced, non-overlapping distance classes.

The covariogram $\hat{C}(h)$ estimates the covariance between residuals as a function of the distance separating them. In the presence of positive spatial autocorrelation, $\hat{C}(h)$ is positive for small h and declines toward zero as h increases. Beyond a certain distance, residuals are approximately uncorrelated and $\hat{C}(h)$ fluctuates around zero.

3.2 The Proposed Bandwidth Selector

I propose to use the empirical covariogram to estimate the *range* of spatial dependence in the regression residuals. This estimated range then serves as the bandwidth for computing spatial HAC standard errors.

Proposition 1 (Covariogram Range Estimator). *Let $\{h_b\}_{b=1}^B$ denote the bin centers at which the empirical covariogram $\hat{C}(\cdot)$ is evaluated. Define the covariogram range estimator as*

$$\hat{\zeta} = \min\{h_b : |\hat{C}(h_b)| \leq \eta\}, \quad (5)$$

where $\eta \geq 0$ is a small tolerance to account for sampling noise. The estimator $\hat{\zeta}$ identifies the shortest distance at which the magnitude of the estimated residual covariance falls below the tolerance band.

In practice, $\hat{C}(h)$ is evaluated at a fixed set of equally spaced, non-overlapping distance bins. Setting $\eta = 0$, the estimator selects the first bin center at which the empirical covariogram crosses zero. For

covariance functions that decay gradually rather than reaching zero exactly (see Remark 4 below), a small positive η can be used; in the Monte Carlo experiments, the default $\eta = 0$ performs well because the binned covariogram is sufficiently noisy that it crosses zero near the effective range.

Remark 1. *The covariogram and the semivariogram are related by $C(h) = C(0) - \gamma(h)$, where $C(0)$ is the variance at distance zero (the "nugget" plus "sill" in geostatistical terminology) and $\gamma(h)$ is the semivariogram. Both convey equivalent information about the spatial correlation structure. The covariogram is used here because the range—the distance at which $C(h)$ crosses zero—has a direct interpretation as the bandwidth beyond which residuals are uncorrelated.*

3.3 Formal Assumptions and Consistency

This section provides sufficient conditions under which the covariogram range estimator $\hat{\zeta}$ is consistent for the true correlation range and the resulting plug-in spatial HAC estimator is consistent for the variance of $\hat{\beta}$. The conditions are stated at a level that makes transparent what is required; a fully detailed proof in the increasing-domain asymptotic framework is beyond the scope of this paper. The Monte Carlo evidence in Section 7 provides the primary validation that the method works in finite-sample settings calibrated to empirically relevant spatial configurations.

Assumption 1 (Stationarity and Mixing). *The error process $\{\varepsilon(\mathbf{s}) : \mathbf{s} \in \mathcal{S}\}$ is second-order stationary: $E[\varepsilon(\mathbf{s})] = 0$ for all \mathbf{s} , and $Cov(\varepsilon(\mathbf{s}_i), \varepsilon(\mathbf{s}_j)) = C(\|\mathbf{s}_i - \mathbf{s}_j\|)$ depends only on the distance $\|\mathbf{s}_i - \mathbf{s}_j\|$ (isotropy). The process satisfies a spatial α -mixing condition with mixing coefficients $\alpha(k)$ satisfying $\sum_{k=1}^{\infty} k^{d-1} \alpha(k)^{\delta/(4+\delta)} < \infty$ for dimension $d = 2$. Additionally, $E[|\varepsilon(\mathbf{s})|^{4+\delta}] < \infty$ for some $\delta > 0$.*

The mixing and moment conditions are needed because pairs of residual products $\hat{\varepsilon}_i \hat{\varepsilon}_j$ sharing common locations are dependent; they ensure a law of large numbers for the binned covariogram averages, which does not follow from the growth in the number of pairs $|N(h)|$ alone.

Assumption 2 (Compact Support and Identification). *There exists a finite $\varsigma_0 > 0$ such that $C(h) = 0$ for all $h > \varsigma_0$. The covariance function satisfies the separation condition:*

$$\text{for every } \delta > 0, \quad \inf_{h \leq \varsigma_0 - \delta} |C(h)| > 0 \quad \text{and} \quad \sup_{h \geq \varsigma_0 + \delta} |C(h)| = 0. \quad (6)$$

Additionally, $C(h)$ is continuous at ς_0 .

The separation condition ensures that the true range ς_0 is well-identified: the covariance is bounded away from zero inside the range and exactly zero outside. This rules out pathological cases where $C(h)$ is “flat” near ς_0 , which would make the threshold crossing unstable under small estimation errors. Note that $C(h)$ need not be positive for all $h < \varsigma_0$ —it may be negative at some distances (e.g., due to oscillatory behavior or residualization)—but it must be nonzero.

Assumption 3 (Increasing-Domain Sampling). *The observation locations $\{\mathbf{s}_1, \dots, \mathbf{s}_n\}$ are sampled in an increasing-domain framework: the spatial region \mathcal{S}_n expands as $n \rightarrow \infty$, with minimum inter-point separation bounded away from zero. The number of pairs $|N(h)|$ in each distance bin grows to infinity for all $h \leq \varsigma_0 + c$ for some $c > 0$.*

This is consistent with the asymptotic framework of [Conley \[1999\]](#) and [Kelejian and Prucha \[2007\]](#), where spatial HAC consistency is established under increasing-domain asymptotics. The condition that $|N(h)| \rightarrow \infty$ across the relevant range of distances ensures that the binned covariogram averages converge.

Assumption 4 (Regularity). *The regressors \mathbf{x}_i are bounded, and the conditions of [@Conley1999](#) and [@KelejianPrucha2007](#) for the consistency of the spatial HAC estimator are satisfied with bandwidth ς_0 . The kernel $K(\cdot)$ is continuous and has compact support (i.e., it is one of the smooth kernels defined in [@sec-kernels-main](#), such as Bartlett or Epanechnikov).*

The kernel continuity requirement ensures that the mapping from bandwidth to the SHAC variance estimate, $\varsigma \mapsto \hat{V}_{\text{SHAC}}(\varsigma)$, is continuous: adding or removing pairs near the cutoff boundary produces only a negligible change in the estimate, because their kernel weights are near zero.

Proposition 2 (Consistency of the Covariogram Range Estimator). *Under Assumptions 1–4, the covariogram range estimator $\hat{\varsigma}$ converges in probability to ς_0 as $n \rightarrow \infty$. Consequently, the spatial HAC estimator \hat{V}_{SHAC} computed with bandwidth $\hat{\varsigma}$ is consistent for the true variance of $\hat{\beta}$.*

Sketch of argument. Let $\{h_b\}_{b=1}^B$ be the fixed bin centers covering $[0, \varsigma_0 + c]$. Under Assumptions 1 and 3, the mixing and moment conditions ensure a law of large numbers for the dependent pairwise

averages within each bin, yielding $\hat{C}(h_b) \rightarrow_p C(h_b)$ for each b . Since B is finite, joint convergence holds, and the maximum over bins converges:

$$\max_{b \leq B} |\hat{C}(h_b) - C(h_b)| \rightarrow_p 0.$$

Because $\hat{C}(h)$ is defined as a piecewise-constant function on the bins, this is equivalent to uniform convergence over the interval. Given this and the separation condition in Assumption 2, the estimator $\hat{\varsigma}$ converges to ς_0 : for any $\delta > 0$, eventually $|\hat{C}(h_b)|$ is bounded away from zero (and hence above η) for all bins $h_b \leq \varsigma_0 - \delta$, and $|\hat{C}(h_b)|$ is close to zero (and hence below η) for all bins $h_b \geq \varsigma_0 + \delta$. Thus the first bin at which $|\hat{C}(h_b)| \leq \eta$ must fall in $(\varsigma_0 - \delta, \varsigma_0 + \delta)$, giving $\hat{\varsigma} \rightarrow_p \varsigma_0$. The second claim follows from the kernel continuity in Assumption 4—which ensures $\hat{V}_{\text{SHAC}}(\hat{\varsigma}) - \hat{V}_{\text{SHAC}}(\varsigma_0) \rightarrow_p 0$. Specifically, under increasing-domain sampling, the number of observation pairs in a thin boundary shell $(\varsigma_0 - \epsilon, \varsigma_0 + \epsilon)$ grows at most proportionally to ϵ , so with a continuous compact-support kernel the marginal contribution of these pairs to $\hat{\cdot}$ vanishes as $\epsilon \downarrow 0$. Combined with the consistency of $\hat{V}_{\text{SHAC}}(\varsigma_0)$ established by Kelejian and Prucha [2007], this yields the result.

Remark 2. *The stationarity assumption rules out spatial trends and non-stationary spatial processes. In practice, non-stationarity can be addressed by including location controls (e.g., coordinates as regressors) or by detrending before applying the covariogram method. The Monte Carlo experiments in @sec-montecarlo include specifications both with and without location controls.*

Remark 3. *The compact support assumption (Assumption 2) is a modeling approximation. It is exactly satisfied by the Spherical covariance model but not by the Exponential or Matérn, whose covariances decay to zero asymptotically without reaching it in finite distance. In practice, these models have an “effective range”—the distance at which the covariance falls below approximately 5% of its sill value—and the covariogram estimator targets this effective range. Formally, one could replace ς_0 with the pseudo-true parameter $\varsigma_0 := \sup\{h : |C(h)| > \eta\}$ for a small threshold $\eta > 0$, and the argument above would carry through with the separation condition stated relative to this threshold. Under compact support, the SHAC estimator is consistent at the true cutoff ς_0 , and the covariogram range provides a consistent estimate of this cutoff. Under decaying covariance without compact support, the covariogram range targets a fixed effective range that serves as a practical bandwidth; formal rate-optimality in that regime is left for future work.*

3.4 Implementation

The proposed method is computationally efficient. The empirical covariogram is computed using the `variogram()` function from `gstat` [Pebesma, 2004] with the `covariogram = TRUE` option. The distance bins are determined by two parameters: `width` (the bin width 2δ) and `cutoff` (the maximum distance). As a default, the bin width is set to ensure approximately 100–200 distance bins up to two-thirds of the maximum inter-point distance. The range is then extracted as the first distance at which the empirical covariogram crosses zero. For a typical dataset with several thousand observations, the entire procedure takes a fraction of a second.

Figure 2 illustrates the method on four simulated datasets with increasing degrees of spatial autocorrelation.

3.5 Connection to Fixed- b Asymptotics

The covariogram-range bandwidth selector has a useful conceptual connection to the fixed- b asymptotic framework. In the classical time-series setting, two asymptotic regimes govern the behavior of HAC standard errors. Under the traditional *small- b* asymptotics of Andrews [1991] and Newey and West [1987], the bandwidth M grows with the sample size T but satisfies $M/T \rightarrow 0$, so that the HAC estimator is consistent and the t -statistic converges to a standard normal. Under the *fixed- b* asymptotics of Kiefer et al. [2000] and Sun et al. [2008], the bandwidth satisfies $M/T \rightarrow b \in (0, 1]$, so the HAC estimator is inconsistent but the resulting test statistic converges to a non-standard distribution that provides more accurate finite-sample size control. Sun [2014] argues that fixed- b inference is generally preferable, as it accounts for the estimation uncertainty in the HAC estimator itself. Bester et al. [2016] extend fixed- b theory to the spatial setting: when the Conley bandwidth grows proportionally with the diameter of the spatial domain—i.e., $\varsigma/\text{diam}(S_n) \rightarrow b > 0$ —the SHAC estimator converges to a nondegenerate random matrix rather than the true variance, and the t -statistic has a non-standard pivotal limit distribution whose critical values must be obtained by simulation.

While the covariogram-range selector does not implement spatial fixed- b inference, it shares the key practical intuition that motivates the fixed- b literature: smoothing should be anchored to the scale of dependence rather than shrinking relative to the sample. The estimator $\hat{\varsigma}$ targets a fixed physical quantity—the correlation range ς_0 —determined entirely by the spatial dependence

structure of the data-generating process. Unlike MSE-optimal rules [e.g., [Andrews, 1991](#)], where the bandwidth grows with T but satisfies $M/T \rightarrow 0$ and tends to undersmooth in finite samples, the covariogram-range bandwidth does not depend on n and is instead pinned to the dependence scale. This fixed-span behavior—anchoring to a physical quantity rather than to sample size—reduces the usual smoothing trade-off that [Sun \[2014\]](#) identifies as the primary source of size distortions in HAC inference.

Formally, however, the covariogram-range method operates in a different asymptotic regime. Under the increasing-domain asymptotics used throughout this paper, a fixed physical bandwidth implies $\varsigma_0/\text{diam}(S_n) \rightarrow 0$, placing the covariogram-range selector in the small- b regime of [Bester et al. \[2016\]](#), not the fixed- b regime. Moreover, under compact support (Assumption 2), the covariance is literally zero beyond ς_0 , so there is no “missing tail” to truncate—unlike the spatial fixed- b setting of [Bester et al. \[2016\]](#), where the bandwidth truncates a non-negligible portion of the dependence structure and the SHAC estimator converges to a nondegenerate random limit. At the true cutoff ς_0 , the SHAC estimator captures the entire covariance structure without truncation bias and is therefore consistent. The plug-in bandwidth $\hat{\varsigma}$ converges to ς_0 , standard SHAC consistency obtains, and no non-standard critical values or simulated reference distributions are required. The finite-sample size improvements documented in Section 7 arise not from the fixed- b mechanism of embracing estimator randomness, but from targeting the correct dependence scale directly—avoiding the undersmoothing that plagues MSE-optimal bandwidth selectors. Nevertheless, in any finite spatial sample the bandwidth-to-domain ratio is a non-negligible constant, so the resulting smoothing can resemble the larger-smoothing behavior that motivates fixed- b corrections.

4 Simulation Design

To evaluate the proposed bandwidth selector, I require spatially correlated random variables with precisely controlled correlation ranges. I generate these using unconditional geostatistical simulation (simple kriging) with the `gstat` package [[Pebesma, 2004](#)]; see [Cressie \[1993\]](#) for a comprehensive treatment of the geostatistical framework. The full details of the simulation procedure—including the kriging system, semivariogram specifications, and implementation—are provided in Section 11.3.

4.1 Spatial Samples

Four spatial samples are used throughout the study, all covering the bounding box of the contiguous United States:

1. **Counties** ($n = 3,108$): Centroids of all counties in the contiguous 48 states. This is a sample with highly unequal spacing between observations.
2. **Coarse lattice** ($n \approx 2,600$): A regular square grid with 70 km cell size.
3. **Medium lattice** ($n \approx 5,096$): A regular square grid with 50 km cell size.
4. **Fine lattice** ($n \approx 10,320$): A regular square grid with 35 km cell size.

The three lattice samples provide controlled variation in sample density, while the county centroid sample tests performance under highly irregular spacing.

4.2 Monte Carlo Design

In each simulation iteration:

1. Two independent spatially correlated random fields are drawn using the procedure described above and in Section 11.3, both with the same range parameter. The first provides the dependent variable y_i (labeled `noise1`) and the second provides the regressor x_i (labeled `noise2`).
2. Each observation is assigned the value of the underlying random field at its location.
3. A univariate regression of y_i on x_i is estimated. Because the two fields are drawn independently, the true coefficient is zero ($\beta = 0$). The t -statistics using HC1 standard errors and using Conley standard errors with various kernel and bandwidth combinations are recorded.
4. The false positive rate is defined as the fraction of simulations in which the null hypothesis $H_0 : \beta = 0$ is rejected at the 5% level using the critical value of 1.96.

This process is repeated for noise range parameters starting from 0 (no spatial correlation) in 15 sequential increments until extreme degrees of spatial correlation are reached, with 5,000 iterations per configuration. The noise range parameter governs the input to the semivariogram; the *realized* correlation range varies stochastically across draws. Computations were carried out on the Akropolis cluster at the University of Chicago using `Rmpi` for parallel processing [R Core Team, 2025]. To

ensure exact replicability, the pseudo-random number seed was set using `clusterSetRNGStream()` with Pierre L’Ecuyer’s `RngStreams` [L’Ecuyer, 1999] (seed: 1908).

For each simulation, the following standard errors are computed:

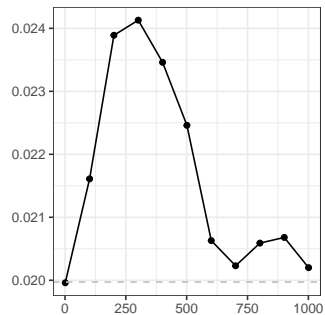
- **HC1**: The standard heteroskedasticity-robust estimator (benchmark).
- **Conley, covariogram-range bandwidth** ($\hat{\zeta}$): The proposed method, computed with six different kernels.
- **Conley, fixed narrow bandwidth** (25 km): A deliberately small bandwidth.
- **Conley, fixed wide bandwidth** (2,500 km): A deliberately large bandwidth representing the “conservative wide bandwidth” advice.

5 The Inverse-U Relationship

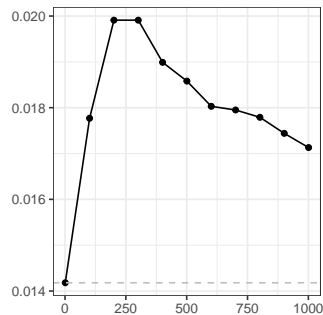
Figure 1 displays the relationship between the kernel bandwidth and the magnitude of Conley standard errors for a single realization of a spatially correlated random field across the four spatial samples. The pattern is striking and consistent: the standard error first *increases* as the bandwidth grows from zero (at which point the Conley SE equals the HC1 SE), reaches a maximum near the true correlation range, and then *decreases* steadily. The method proposed in this paper always picks the peak of this inverse-U curve as the standard error.

This inverse-U shape has immediate practical consequences. Starting from a narrow bandwidth, expanding the range over which residuals are allowed to be correlated initially leads to larger standard errors—as expected, since positive residual correlation adds to the estimated variance. However, beyond the range of actual correlation, additional observations included in the kernel contribute only noise to the variance estimate: their cross-products $\hat{\varepsilon}_i \hat{\varepsilon}_j$ have expectation zero but dilute the positive contributions from truly correlated pairs. As the bandwidth continues to grow, this dilution effect dominates and the standard error declines.

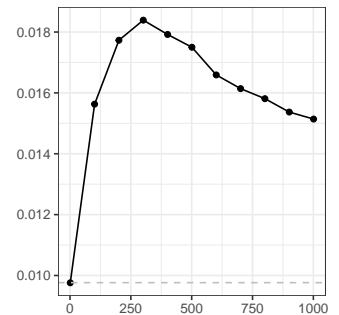
For very wide bandwidths, the standard error can fall *below* the HC1 level. This directly contradicts the conventional wisdom that wider bandwidths ensure conservative inference. In fact, choosing a bandwidth much larger than the true correlation range can lead to standard errors that are *smaller* than even the heteroskedasticity-only estimator, resulting in overrejection that exceeds even the overrejection from ignoring spatial correlation entirely.



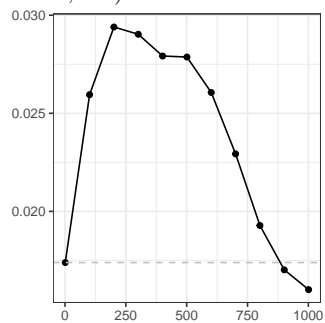
(a) Coarse lattice ($n \approx 2,600$).



(b) Medium lattice ($n \approx 5,096$).



(c) Fine lattice ($n \approx 10,320$).



(d) County centroids ($n = 3,108$).

Figure 1: The inverse-U relationship between the magnitude of spatial HAC standard errors and the kernel bandwidth for all four samples. Each panel uses a single realization of a spatially correlated random field (Mat'ern, range 50 km). The dashed grey line indicates the corresponding HC1 standard error. It can be seen that overly wide bandwidths drive the size of the Conley standard error down to the levels of the HC1 standard error with overly inflated t-stats.

The practical implication is clear: the bandwidth should be matched to the actual range of spatial correlation in the residuals. This is precisely what the covariogram range method proposed in Section 3 achieves.

6 Illustrating the Covariogram Range Method

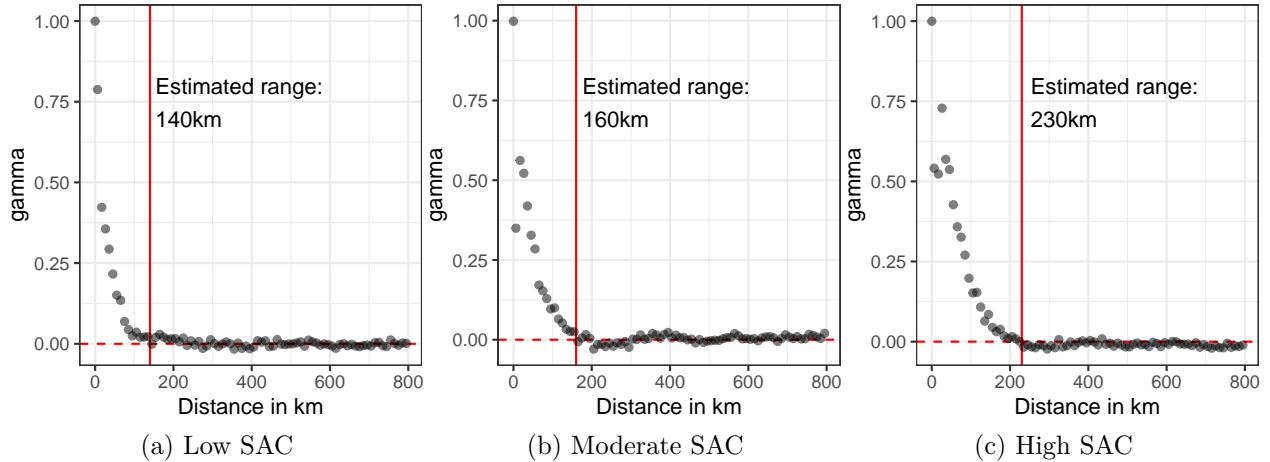


Figure 2: Empirical covariograms of regression residuals from univariate regressions of two independently drawn spatial noise fields, estimated on 3,108 county centroids. The red vertical line indicates the estimated correlation range $\hat{\zeta}$. This corresponds to the peak of the inverse-U curve illustrated earlier. The red dashed horizontal line marks zero covariance.

Figure 2 visualizes the covariogram range method on three regression residual series with increasing degrees of spatial autocorrelation. In each panel, the empirical covariogram declines from a positive value at short distances and crosses zero at the estimated range $\hat{\zeta}$ (marked by the red vertical line). Beyond $\hat{\zeta}$, the covariogram fluctuates around zero, indicating the absence of residual correlation. As the degree of spatial autocorrelation increases from panel (a) to (c), the estimated range shifts rightward, correctly tracking the growing extent of spatial dependence.

7 Monte Carlo Results

7.1 Main Results: Size Control

Table 1 presents the main results across the three regular lattice samples. The covariogram-range method with the Epanechnikov kernel consistently maintains rejection rates near 5% across all

[!h]

Noise #	$n = 2,600$ (70km grid)			$n = 5,096$ (50km grid)			$n = 10,320$ (35km grid)		
	Range	HC1	Epan.	Range	HC1	Epan.	Range	HC1	Epan.
0	143	5.2	5.2	109	4.9	5.1	83	4.8	4.9
1	141	4.6	4.7	98	4.5	4.5	83	4.7	4.7
2	131	4.9	4.9	140	5.0	4.8	150	7.1	5.3
3	178	6.1	5.7	209	7.2	5.5	226	13.6	6.1
4	231	7.1	5.6	267	12.3	6.1	295	21.5	5.8
5	284	9.2	5.5	324	17.0	6.0	355	29.9	6.3
6	335	13.7	6.4	370	23.2	6.4	406	38.9	6.5
7	382	17.7	6.5	421	29.6	6.4	451	46.3	6.6
8	429	22.0	6.9	468	36.2	6.9	500	50.8	6.7
9	472	25.6	6.6	509	40.4	6.8	537	54.8	7.2
10	510	30.6	7.4	551	45.5	7.8	581	60.0	7.5
11	540	35.5	7.9	579	49.1	8.4	604	62.8	8.3
12	576	38.8	8.0	619	51.4	8.5	647	65.5	8.4
13	614	42.0	8.7	654	55.7	8.7	678	68.0	8.5
14	639	45.2	9.1	679	57.9	9.0	702	69.4	8.9
15	660	47.7	8.5	701	60.0	8.8	722	71.6	9.2

Table 1: Null rejection frequencies (%) of nominal 5% level tests for linear regressions using the three regular lattice samples. The table juxtaposes HC1 standard errors with spatial HAC standard errors using the introduced covariogram-range bandwidth and an Epanechnikov kernel. Results based on 5,000 Monte Carlo simulations for every range-sample pair. The range column illustrates the increasing degree of spatial correlation as the range of the simulated spatial fields increases. As can be seen from the overly inflated HC1 rejection rates, the last few rows of the table showcase unrealistically high scenarios of spatial correlation. Despite that, the proposed method reduces a rejection rate of over 70% to around 9%.

[!h]

Noise #	Range (km)	HC1	Fixed bandwidth		Covariogram range		
			Fixed 25km	Fixed 2500km	Bartlett	Uniform	Epan.
0	49	4.8	4.7	24.4	4.8	5.1	4.9
1	72	5.1	5.0	23.6	4.9	5.0	4.9
2	130	6.7	6.3	24.6	5.6	5.5	5.4
3	189	11.6	10.5	25.5	6.4	6.5	6.1
4	243	18.1	16.3	26.8	7.8	7.5	7.2
5	287	25.2	23.0	27.8	8.3	7.9	6.9
6	324	32.8	30.4	29.4	9.3	9.0	7.7
7	360	37.1	34.7	30.2	9.6	9.3	8.2
8	386	43.5	40.5	30.1	10.8	10.1	9.1
9	418	47.3	44.4	30.1	11.3	11.2	9.5
10	445	52.7	49.8	30.4	11.5	11.0	9.7
11	464	56.6	54.2	31.9	13.0	12.3	11.0
12	484	58.0	55.5	30.7	13.2	13.0	11.5
13	506	61.2	59.0	31.6	14.2	13.2	12.0
14	523	64.5	62.2	31.9	14.9	14.6	12.8
15	529	64.4	62.0	32.1	14.6	14.2	12.1

Table 2: Null rejection frequencies (%) of nominal 5% level tests for linear regressions for the county centroid sample ($n = 3,108$). The table juxtaposes HC1 standard errors with spatial HAC standard errors using the introduced covariogram-range bandwidth (showcasing the rejection frequencies of the Bartlett, Uniform, and Epanechnikov kernel next to each other). The fixed bandwidth columns illustrate the failure of both too narrow and too wide cutoff bandwidths for the spatial HAC standard error estimate after Conley (1999). Results based on 5,000 Monte Carlo simulations for every noise range grouping. The range column illustrates the increasing degree of spatial correlation as the range of the simulated spatial fields increases. As can be seen from the overly inflated HC1 rejection rates, the last few rows of the table showcase unrealistically high scenarios of spatial correlation.

sample sizes and spatial configurations, while HC1 rejection rates rise sharply with spatial autocorrelation. Larger samples ($n = 10,320$) tend to produce slightly more accurate size control, consistent with the consistency result in Proposition 2.

Table 2 presents the detailed results for the county centroid sample ($n = 3,108$). Several findings stand out.

First, HC1 standard errors lead to substantial overrejection as spatial autocorrelation increases. At the highest noise ranges, the false positive rate exceeds 60%, far above the nominal 5%.

Second, a fixed narrow bandwidth of 25 km offers no improvement over HC1 when the true correlation range exceeds this bandwidth. Conversely, a fixed wide bandwidth of 2,500 km—meant to be “conservative”—also fails to control size, confirming the inverse-U prediction: at very wide

bandwidths, the standard error is deflated below the HC1 level.

Third, the proposed covariogram-range method with Bartlett, Uniform, or Epanechnikov kernels controls the rejection rate remarkably well. Across all noise range configurations, the false positive rate remains close to the nominal 5%. At the most extreme degrees of spatial autocorrelation (with noise ranges far above empirically realistic levels), the rejection rate rises to approximately 8–10%, reflecting the inherent difficulty of spatial HAC estimation when the correlation range approaches a substantial fraction of the spatial domain.

Taken together, the results demonstrate that the covariogram-range bandwidth selector provides effective size control across the empirically relevant spectrum of spatial dependence. For the correlation ranges most commonly encountered in applied work—where HC1 rejection rates already exceed 15–30%—the proposed method maintains false positive rates in the range of 5–8%, close to the nominal level. The modest overrejection observed at extreme correlation ranges reflects a regime that pushes far beyond what typical georeferenced datasets exhibit, and even there the covariogram-range method substantially outperforms all fixed-bandwidth alternatives.

7.2 Kernel Comparison

Table 3 reports rejection frequencies for all six kernel functions. The Bartlett and Epanechnikov kernels consistently deliver rejection rates closest to the nominal 5% level. The Uniform kernel performs well at moderate spatial autocorrelation but tends to slightly overreject at high levels. The Gaussian, Parzen, and Quartic Biweight kernels show somewhat more variable performance, with a tendency toward overrejection at higher noise ranges. Based on these results, I recommend the **Bartlett** or **Epanechnikov** kernel for applied work, consistent with the time-series finding of [Kolokotronis et al. \[2024\]](#) regarding the optimality of Bartlett among first-order kernels.

7.3 Visual Summary

Figure 3 provides a visual summary of the results presented in Table 1 and Table 2, plotting every individual simulation run and illustrating how false rejection rates increase with the degree of spatial correlation. Each column corresponds to one of the four spatial samples; each row to a different standard error type. The top row (HC1) shows that t -statistics grow with the correlation range when both the outcome and regressor are spatially correlated, producing the

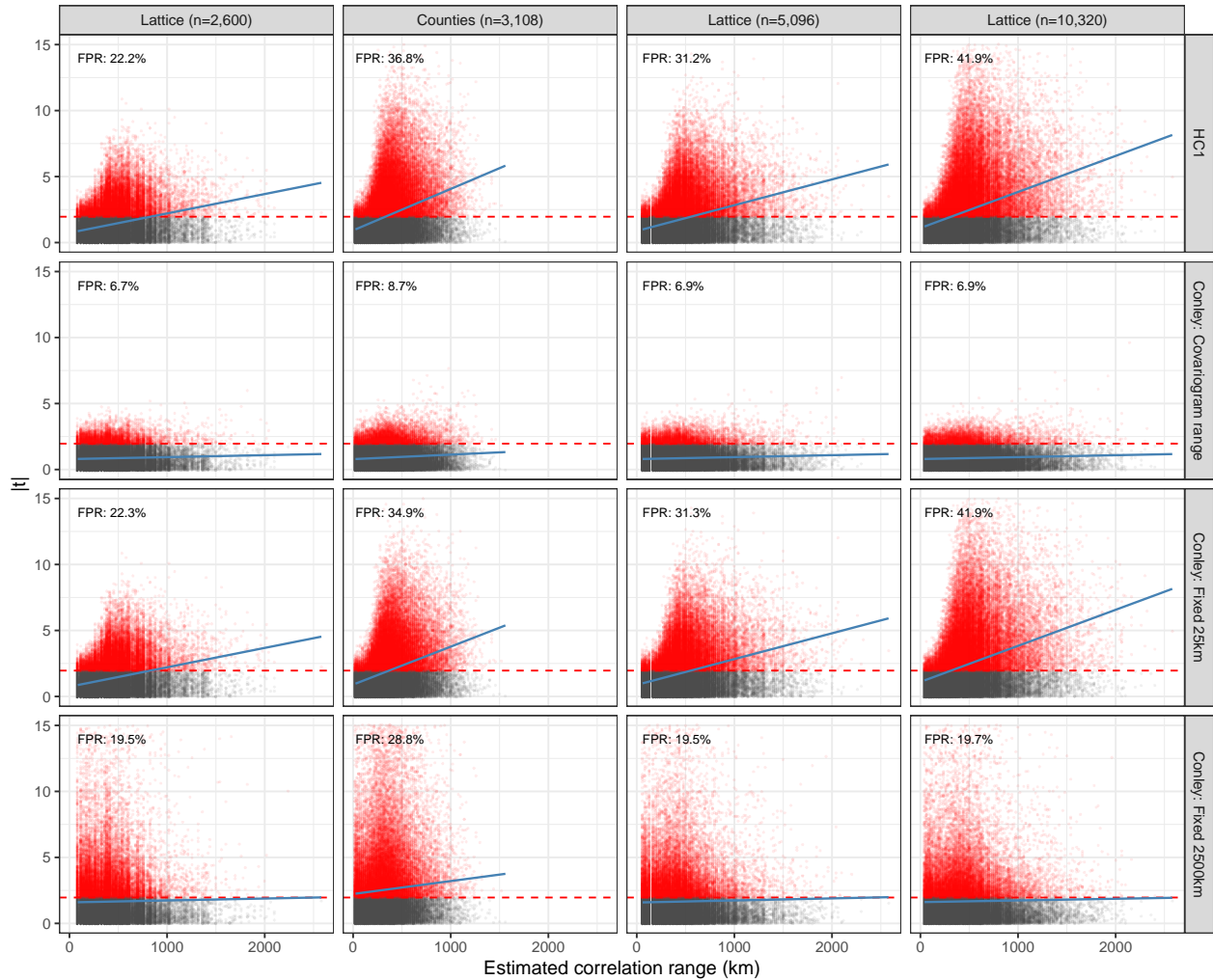


Figure 3: Visual summary of the simulation results in tables 1 and 2. Absolute t -statistics from 5,000 Monte Carlo simulations plotted against the estimated correlation range. Each dot is one simulation. Red dots indicate rejections ($|t| > 1.96$). The annotation shows the false positive rate (FPR) across the entire sample. Columns correspond to the four spatial samples; rows compare HC1, spatial HAC errors using the proposed covariogram-range bandwidth estimator (Epanechnikov kernel), a fixed narrow bandwidth (25 km), and a fixed wide bandwidth (2,500 km). The blue line indicates a regression line showing the decreasing performance of conventional errors as the degree of spatial correlation increases. It can be visually inferred that the proposed method provides reasonable size control even for extreme degrees of spatial correlation

[!h]

Noise #	Bartlett	Uniform	Epan.	Gaussian	Parzen	Biweight
0	4.9	5.0	5.1	5.0	4.8	5.0
1	4.5	4.8	4.5	4.7	4.5	4.5
2	4.9	5.1	4.8	5.0	4.9	4.9
3	5.9	5.6	5.5	5.6	5.9	5.6
4	6.8	6.2	6.1	6.2	7.0	6.3
5	7.2	6.0	6.0	6.0	7.5	6.4
6	7.6	6.7	6.4	6.6	7.8	6.6
7	8.0	7.0	6.4	6.6	8.4	6.7
8	8.7	7.3	6.9	7.1	8.7	7.5
9	8.5	7.3	6.8	7.1	8.5	7.2
10	9.4	8.2	7.8	7.9	9.6	7.9
11	10.2	9.0	8.4	8.6	10.5	8.6
12	10.4	9.2	8.5	8.7	10.7	8.7
13	10.8	9.8	8.7	9.4	10.9	8.9
14	10.8	10.3	9.0	9.9	10.8	8.9
15	10.9	10.0	8.8	9.7	11.3	9.1

Table 3: Null rejection frequencies (%) by kernel function using the covariogram-range bandwidth. Regular lattice sample ($n = 5,096$, 50km grid). Results based on 5,000 simulations per configuration.

substantial overrejection documented in the tables. The second row demonstrates the covariogram-range method: the t -statistics remain centered below the critical value regardless of the correlation range, with approximately 5% of dots exceeding the threshold. The third and fourth rows show the failure modes of fixed bandwidths: a narrow bandwidth (25 km) behaves like HC1 when the true range exceeds 25 km, and a wide bandwidth (2,500 km) deflates standard errors and produces high rejection rates across the board.

8 Empirical Application

To illustrate the practical relevance of the proposed method, I apply it to a regression using U.S. county-level data. The outcome variable is the share of the Black population in each county, and the regressor is the share of the Hispanic population—two variables that exhibit well-known spatial clustering patterns across the United States. The data is from the latest US census, accessed through IPUMS [Ruggles et al., 2025].

Table 4 presents the results. The HC1 standard error is the smallest, producing the largest t -statistic. The Conley standard errors vary substantially with the bandwidth choice. At the estimated covar-

Table 4: Empirical application: Regression of Black population share on Hispanic population share across 3,108 U.S. counties. Standard errors in parentheses. Conley standard errors computed using the Epanechnikov kernel.

[!h]

Standard error type	Coefficient	SE	<i>t</i> -statistic
HC1	-0.1168	0.0101	-11.51
Conley (25 km)	-0.1168	0.0105	-11.10
Conley (980 km, $\hat{\zeta}$)	-0.1168	0.0884	-1.32
Conley (500 km)	-0.1168	0.0766	-1.53
Conley (2500 km)	-0.1168	0.0561	-2.08

igram range of approximately 980 km, the standard error is the largest among all choices shown, consistent with the inverse-U pattern. This is the appropriate bandwidth for this regression: the estimated range reflects the spatial extent of residual correlation in these demographic variables. At bandwidths of 500 km and 2,500 km—which might seem “safer” to an applied researcher—the standard errors are actually smaller, illustrating precisely the misleading effect documented in Section 5.

This example demonstrates a scenario commonly encountered in applied spatial research: widely used variables with strong spatial clustering patterns that extend over large distances. The covariogram range method correctly identifies this extent and produces appropriately sized standard errors.

9 Conclusion

This paper addresses the unresolved problem of bandwidth selection for spatial HAC standard errors. I make three main contributions.

First, I document that the relationship between the kernel bandwidth and the magnitude of spatial HAC standard errors follows an inverse-U shape. This implies that both too narrow *and* too wide bandwidths lead to underestimated standard errors. The finding contradicts the common advice that wider bandwidths are more conservative and establishes that the bandwidth choice is not merely a matter of being “generous” with the cutoff distance.

Second, I propose a simple, non-parametric bandwidth selector based on the empirical covariogram of regression residuals. The estimator identifies the distance at which residual covariation first

crosses zero—the correlation range—and uses this as the bandwidth for the spatial HAC estimator. Under standard regularity conditions, the estimator is consistent for the true correlation range.

Third, I show through extensive Monte Carlo simulations that the proposed method controls the false positive rate at or near the nominal 5% level across a wide range of spatial autocorrelation intensities and sample configurations. A systematic comparison of six kernel functions finds that the Bartlett and Epanechnikov kernels deliver the best size control, extending the time-series finding of [Kolokotronis et al. \[2024\]](#) to the spatial domain. At extreme levels of spatial correlation, where the correlation range approaches a substantial fraction of the spatial domain, the rejection rate rises to approximately 8–10%. This residual overrejection should be understood as a fundamental limitation of spatial inference under very strong dependence rather than a failure of the proposed selector: when effective degrees of freedom become small, no HAC-type estimator—whether based on fixed bandwidths, cluster-robust methods, or data-driven selection—performs well. The key result is comparative: across all configurations considered, the covariogram-range method substantially improves size control relative to HC1, fixed narrow bandwidths, and fixed wide bandwidths.

The proposed method is implemented in the R package `SpatialInference`.

9.1 Declaration of generative AI and AI-assisted technologies in the manuscript preparation process

During the preparation of this work the author used Claude (Anthropic) in order to assist with manuscript drafting. After using this tool, the author reviewed and edited the content as needed and takes full responsibility for the content of the published article.

10 References

- Donald W. K. Andrews. Heteroskedasticity and Autocorrelation Consistent Covariance Matrix Estimation. *Econometrica*, 59(3):817–858, 1991. doi: 10.2307/2938229.
- Luc Anselin. *Spatial Econometrics: Methods and Models*. Springer Science & Business Media, August 1988. ISBN 978-90-247-3735-2.

- Luc Anselin and Daniel A. Griffith. Do Spatial Effects Really Matter in Regression Analysis? *Papers in Regional Science*, 65(1):11–34, 1988. ISSN 1435-5957. doi: 10.1111/j.1435-5957.1988.tb01155.x. URL <https://rsaiconnect.onlinelibrary.wiley.com/doi/abs/10.1111/j.1435-5957.1988.tb01155.x>.
- Marianne Bertrand, Esther Duflo, and Sendhil Mullainathan. How Much Should We Trust Differences-in-Differences Estimates? *The Quarterly Journal of Economics*, 119(1):249–275, February 2004. doi: 10.1162/003355304772839588.
- C. Alan Bester, Timothy G. Conley, and Christian B. Hansen. Inference with dependent data using cluster covariance estimators. *Journal of Econometrics*, 165(2):137–151, 2011. doi: 10.1016/j.jeconom.2011.01.007.
- C. Alan Bester, Timothy G. Conley, Christian B. Hansen, and Timothy J. Vogelsang. Fixed-b asymptotics for spatially dependent robust nonparametric covariance matrix estimators. *Econometric Theory*, 32(1):154–186, 2016. doi: 10.1017/S0266466614000814.
- Roger Bivand, Micah Altman, Luc Anselin, Renato Assunção, Olaf Berke, Andrew Bernat, Guillaume Blanchet, Eric Blankmeyer, Marilia Carvalho, Bjarke Christensen, Yongwan Chun, Carsten Dormann, Stéphane Dray, Virgilio Gómez-Rubio, Martin Gubri, Rein Halbersma, Elias Krainski, Pierre Legendre, Nicholas Lewin-Koh, Angela Li, Hongfei Li, Jielai Ma, Abhirup Mallik, Giovanni Millo, Werner Mueller, Hisaji Ono, Pedro Peres-Neto, Gianfranco Piras, Markus Reder, Michael Tiefelsdorf, René Westerholt, and Danlin Yu. Spdep: Spatial Dependence: Weighting Schemes, Statistics, June 2020. URL <https://CRAN.R-project.org/package=spdep>.
- A. D. Cliff and J. K. Ord. *Spatial Processes: Models and Applications*. Pion Limited, London, UK, 1981.
- Timothy G. Conley. GMM estimation with cross sectional dependence. *Journal of Econometrics*, 92(1):1–45, September 1999. ISSN 0304-4076. doi: 10.1016/S0304-4076(98)00084-0. URL <http://www.sciencedirect.com/science/article/pii/S0304407698000840>.
- Timothy G. Conley and Morgan Kelly. The Standard Errors of Persistence. *Journal of International Economics*, 153:103986, 2025. doi: 10.1016/j.jinteco.2024.103986.
- Noel Cressie. *Statistics for Spatial Data*. Wiley-Interscience, New York, revised edition edition, September 1993. ISBN 978-0-471-00255-0.

Stefano DellaVigna, Guido Imbens, Woojin Kim, and David Ritzwoller. Using Multiple Outcomes to Adjust Standard Errors for Spatial Correlation. Working Paper 33716, National Bureau of Economic Research, April 2025.

Friedhelm Eicker. Asymptotic Normality and Consistency of the Least Squares Estimators for Families of Linear Regressions. *The Annals of Mathematical Statistics*, 34(2):447–456, June 1963. ISSN 0003-4851, 2168-8990. doi: 10.1214/aoms/1177704156. URL <https://projecteuclid.org/journals/annals-of-mathematical-statistics/volume-34/issue-2/Asymptotic-Normality-and-Consistency-of-the-Least-Squares-Estimators-for/10.1214/aoms/1177704156.full>.

Andrew Gelman and Eric Loken. The garden of forking paths: Why multiple comparisons can be a problem, even when there is no “fishing expedition” or “p-hacking” and the research hypothesis was posited ahead of time. *mimeo, Columbia*, 2013.

Peter J. Huber. The behavior of maximum likelihood estimates under nonstandard conditions. In *Proceedings of the Fifth Berkeley Symposium on Mathematical Statistics and Probability, Volume 1: Statistics*, volume 5.1, pages 221–234. University of California Press, January 1967. URL <https://projecteuclid.org/ebooks/berkeley-symposium-on-mathematical-statistics-and-probability/Proceedings-of-the-Fifth-Berkeley-Symposium-on-Mathematical-Statistics-and/chapter/The-behavior-of-maximum-likelihood-estimates-under-nonstandard-conditions/bsmsp/1200512988>.

Harry H. Kelejian and Ingmar R. Prucha. HAC estimation in a spatial framework. *Journal of Econometrics*, 140(1):131–154, September 2007. ISSN 0304-4076. doi: 10.1016/j.jeconom.2006.09.005. URL <http://www.sciencedirect.com/science/article/pii/S0304407606002260>.

Nicholas M. Kiefer, Timothy J. Vogelsang, and Helle Bunzel. Simple robust testing of regression hypotheses. *Econometrica*, 68(3):695–714, 2000. doi: 10.1111/1468-0262.00128.

Min Seong Kim and Yixiao Sun. Spatial heteroskedasticity and autocorrelation consistent estimation of covariance matrix. *Journal of Econometrics*, 160(2):349–371, February 2011. ISSN 0304-4076. doi: 10.1016/j.jeconom.2010.10.002. URL <http://www.sciencedirect.com/science/article/pii/S0304407610002034>.

Thomas Kolokotronis, James H. Stock, and Christopher D. Walker. Is Newey–West Optimal among First-Order Kernels? *Journal of Econometrics*, 240(2):105696, 2024. doi: 10.1016/j.jeconom.2023.105696.

- Pierre L'Ecuyer. Good Parameters and Implementations for Combined Multiple Recursive Random Number Generators. *Operations Research*, 47(1):159–164, February 1999. ISSN 0030-364X, 1526-5463. doi: 10.1287/opre.47.1.159. URL <https://pubsonline.informs.org/doi/10.1287/opre.47.1.159>.
- Kung-Yee Liang and Scott L. Zeger. Longitudinal data analysis using generalized linear models. *Biometrika*, 73(1):13–22, April 1986. ISSN 0006-3444. doi: 10.1093/biomet/73.1.13. URL <https://doi.org/10.1093/biomet/73.1.13>.
- P. A. P. Moran. The Interpretation of Statistical Maps. *Journal of the Royal Statistical Society. Series B (Methodological)*, 10(2):243–251, 1948. ISSN 0035-9246. URL <https://www.jstor.org/stable/2983777>.
- P. A. P. Moran. Notes on Continuous Stochastic Phenomena. *Biometrika*, 37(1/2):17–23, 1950. ISSN 0006-3444. doi: 10.2307/2332142. URL <https://www.jstor.org/stable/2332142>.
- Brent R. Moulton. Random group effects and the precision of regression estimates. *Journal of Econometrics*, 32(3):385–397, 1986. doi: 10.1016/0304-4076(86)90021-7.
- Ulrich K. Müller and Mark W. Watson. Spatial Correlation Robust Inference. *Econometrica*, 90(6):2901–2935, 2022. ISSN 0012-9682. doi: 10.3982/ECTA19465. URL <https://www.econometricsociety.org/doi/10.3982/ECTA19465>.
- Ulrich K. Müller and Mark W. Watson. Spatial Correlation Robust Inference in Linear Regression and Panel Models. *Journal of Business & Economic Statistics*, 41(4):1050–1064, October 2023. ISSN 0735-0015, 1537-2707. doi: 10.1080/07350015.2022.2127737. URL <https://www.tandfonline.com/doi/full/10.1080/07350015.2022.2127737>.
- Ulrich K. Müller and Mark W. Watson. Spatial Unit Roots and Spurious Regression. *Econometrica*, 92(5):1661–1695, September 2024. doi: 10.3982/ECTA21654.
- Whitney Newey and Kenneth West. A Simple, Positive Semi-definite, Heteroskedasticity and Autocorrelation Consistent Covariance Matrix. *Econometrica*, 55(3):703–08, 1987. URL https://econpapers.repec.org/article/ecmemetrp/v_3a55_3ay_3a1987_3ai_3a3_3ap_3a703-08.htm.
- Edzer J Pebesma. Multivariable geostatistics in S: The gstat package. *Computers & Geosciences*, 30(7):683–691, August 2004. ISSN 0098-3004. doi: 10.1016/j.cageo.2004.03.012. URL <https://www.sciencedirect.com/science/article/pii/S0098300404000676>.

- R Core Team. *R: A Language and Environment for Statistical Computing*. R Foundation for Statistical Computing, Vienna, Austria, 2025. URL <https://www.R-project.org/>.
- Steven Ruggles, Sarah Flood, Matthew Sobek, Daniel Backman, Grace Cooper, Julia A. Rivera Drew, Stephanie Richards, Renae Rogers, Jonathan Schroeder, and Kari C.W. Williams. IPUMS USA: Version 16.0 [dataset], 2025.
- Student. The Elimination of Spurious Correlation due to position in Time or Space. *Biometrika*, 10(1):179–180, April 1914. ISSN 0006-3444. doi: 10.1093/biomet/10.1.179. URL <https://academic.oup.com/biomet/article/10/1/179/189945>.
- Yixiao Sun. Let’s fix it: Fixed-b asymptotics versus small-b asymptotics in heteroscedasticity and autocorrelation robust inference. *Journal of Econometrics*, 178:659–677, 2014. doi: 10.1016/j.jeconom.2013.10.006.
- Yixiao Sun, Peter C. B. Phillips, and Sainan Jin. Optimal bandwidth selection in heteroskedasticity-autocorrelation robust testing. *Econometrica*, 76(1):175–194, 2008. doi: 10.1111/j.0012-9682.2008.00822.x.
- W. R. Tobler. A Computer Movie Simulating Urban Growth in the Detroit Region. *Economic Geography*, 46(sup1):234–240, June 1970. ISSN 0013-0095. doi: 10.2307/143141. URL <https://www.tandfonline.com/doi/abs/10.2307/143141>.
- Halbert White. A Heteroskedasticity-Consistent Covariance Matrix Estimator and a Direct Test for Heteroskedasticity. *Econometrica*, 48(4):817–38, 1980. URL https://econpapers.repec.org/article/ecmemetrp/v_3a48_3ay_3a1980_3ai_3a4_3ap_3a817-38.htm.

11 Appendix

11.1 Details on Spatial HAC Estimation

The spatial HAC estimator in Equation 2 can be written more explicitly. Let $\hat{\varepsilon}_i$ denote the OLS residual for observation i , and let \mathbf{X} be the $n \times p$ regressor matrix. The estimator of the middle term is

$$\hat{\sigma}^2 = \sum_{i=1}^n \sum_{j=1}^n K\left(\frac{d_{ij}}{\varsigma}\right) \hat{\varepsilon}_i \hat{\varepsilon}_j \mathbf{x}_i \mathbf{x}_j',$$

where the double sum runs over all n^2 pairs. In practice, this is computed efficiently by exploiting the sparsity of the kernel: only pairs with $d_{ij} < \varsigma$ contribute non-zero terms. The distance matrix is computed using the Haversine formula when working with geographic (longitude, latitude) coordinates, and Euclidean distance when working with projected coordinates.

The spatial HAC estimator nests several familiar estimators as special cases:

- When $\varsigma = 0$: \hat{V}_{SHAC} reduces to the HC estimator [Eicker, 1963, Huber, 1967, White, 1980].
- When $K(\cdot) = \mathbf{1}(\cdot)$ (Uniform kernel) and ς defines group membership: \hat{V}_{SHAC} reduces to the cluster-robust estimator [Liang and Zeger, 1986, Moulton, 1986].

See Kelejian and Prucha [2007] for a detailed treatment of the asymptotic properties and Bester et al. [2011] for the connection to cluster covariance estimators.

11.2 Spatial Kernel Visualizations

11.3 Generating Spatially Correlated Random Fields

Assume $\mathbf{z}(\mathbf{s}) = (z(\mathbf{s}_1), \dots, z(\mathbf{s}_n))'$ are observations with known mean at spatial locations $\mathbf{s}_1, \dots, \mathbf{s}_n$.

The random process can be written in terms of the classical geostatistical model

$$\mathbf{z}(\mathbf{s}) = \boldsymbol{\mu}(\mathbf{s}) + \mathbf{e}(\mathbf{s}), \tag{7}$$

where $\mathbf{e}(\cdot)$ is a zero-mean random error process with a spatially dependent component modeled by one of the semivariogram functional forms introduced below, so that $E[\mathbf{z}(\mathbf{s})] = \boldsymbol{\mu}(\mathbf{s})$. For simple kriging, the mean is set to zero.

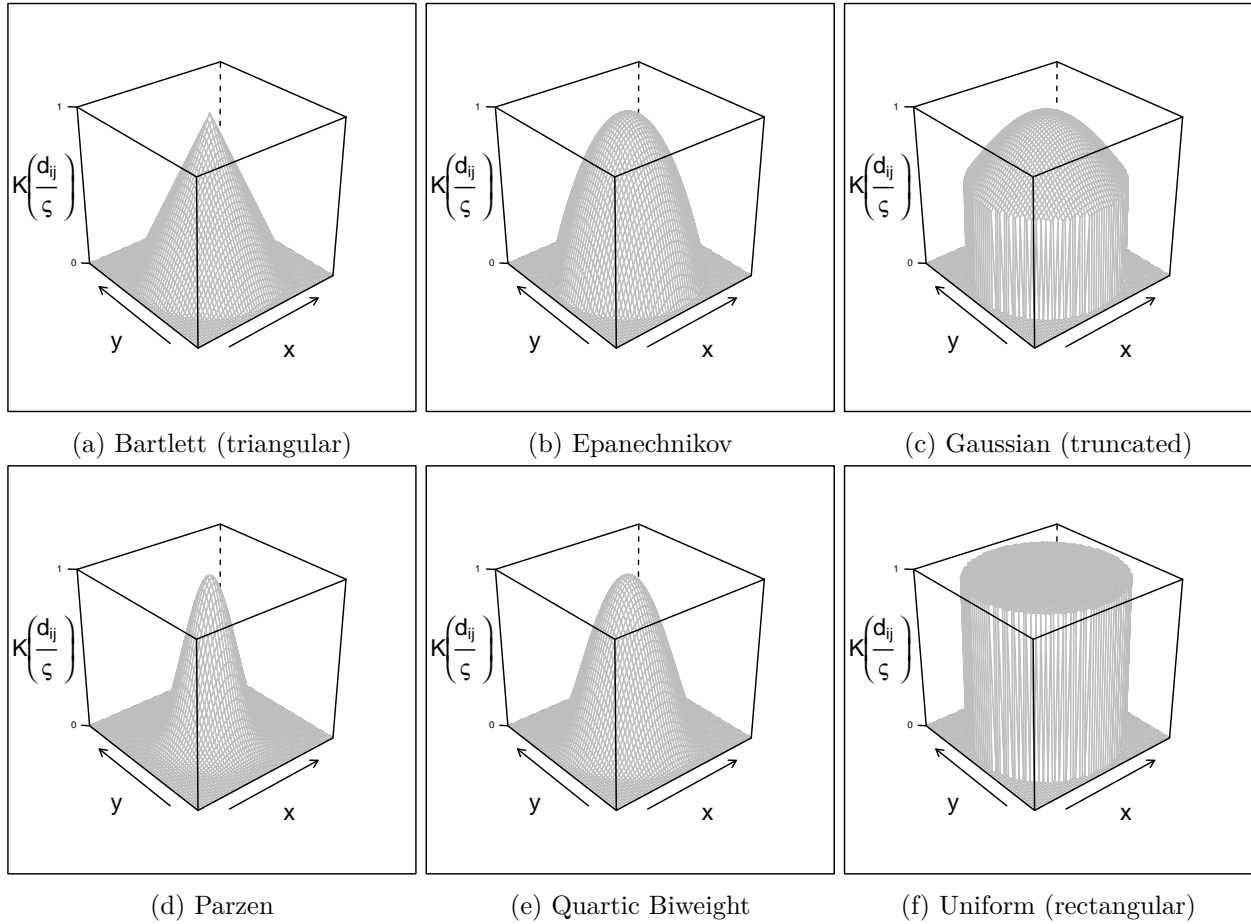


Figure 4: All six two-dimensional kernels used in this study, evaluated on a regular grid. Each panel shows the kernel weight as a function of position relative to the center point.

The goal is to predict the value of z at a new location \mathbf{s}_0 , i.e., to obtain an estimate $\hat{z}(\mathbf{s}_0)$. In ordinary kriging, the predicted value is a weighted linear combination of the observed values:

$$\hat{z}(\mathbf{s}_0) = \sum_{i=1}^n \lambda_i z(\mathbf{s}_i). \quad (8)$$

The weights λ_i are obtained by minimizing the prediction error variance, $\text{Var}[\hat{z}(\mathbf{s}_0) - z(\mathbf{s}_0)]$. It can be shown that solving the following block matrix system yields the optimal weights $\lambda_1, \dots, \lambda_n$ [Cressie, 1993]:

$$\begin{bmatrix} \Gamma & \mathbf{1} \\ \mathbf{1}' & 0 \end{bmatrix} \begin{bmatrix} \lambda \\ m \end{bmatrix} = \begin{bmatrix} \gamma_0 \\ 1 \end{bmatrix}, \quad (9)$$

where Γ is the $n \times n$ matrix with entries $[\Gamma]_{ij} = \gamma(d(\mathbf{s}_i, \mathbf{s}_j))$, and γ_0 is the $n \times 1$ vector with entries $[\gamma_0]_i = \gamma(d(\mathbf{s}_i, \mathbf{s}_0))$. The vector of weights is $\lambda = (\lambda_1, \lambda_2, \dots, \lambda_n)'$ and m is a Lagrange multiplier ensuring $\sum_{i=1}^n \lambda_i = 1$. The vectors $\mathbf{1}$ are of length n .

The defining element of this spatial process is the semivariogram $\gamma(\cdot)$. It determines the semivariance between different pairs of observations that are distance $d(\mathbf{s}_i, \mathbf{s}_j)$ apart:

$$\gamma(d(\mathbf{s}_i, \mathbf{s}_j)) = \frac{1}{2} \text{Var}[z(\mathbf{s}_i) - z(\mathbf{s}_j)]. \quad (10)$$

Note that the relation to the covariogram is $C(\mathbf{h}) = C(\mathbf{0}) - \gamma(\mathbf{h})$, where $C(\mathbf{0})$ denotes the variation at distance zero—referred to as the “nugget effect” in the geostatistical literature. The covariance between points becomes effectively zero at a distance h equal to the range.

The shape of the random spatial process is determined by choosing one of the various valid semivariogram model distance decay functions. For the evaluation of standard error performance, only variations in the range parameter θ_2 matter while everything else is held constant. For completeness, the most commonly used functional forms in geostatistics are:

Table 5: Semivariogram models used in geostatistical simulation. In all specifications, θ_1 is the partial sill and θ_2 is the range parameter.

Model	Semivariogram Specification
Exponential	$\gamma(h; \theta) = \theta_1 \{1 - \exp(-h/\theta_2)\}$
Gaussian	$\gamma(h; \theta) = \theta_1 \{1 - \exp(-h^2/\theta_2^2)\}$

Model	Semivariogram Specification
Mat'{'e}rn	$\gamma(h; \theta) = \theta_1 \left(1 - \frac{(h/\theta_2)^\nu K_\nu(h/\theta_2)}{2^{\nu-1} \Gamma(\nu)} \right)$, where $K_\nu(\cdot)$ is the modified Bessel function of the second kind of order ν and $\Gamma(\cdot)$ is the Gamma function
Spherical	$\gamma(h; \theta) = \begin{cases} \theta_1 \left(\frac{3h}{2\theta_2} - \frac{h^3}{2\theta_2^3} \right) & \text{for } 0 \leq h \leq \theta_2 \\ \theta_1 & \text{for } h > \theta_2 \end{cases}$

The preferred choice in this paper is the Mat'{'e}rn semivariogram, with partial sill $\theta_1 = 0.025$. Results are qualitatively identical with Exponential and Spherical specifications.

In practice, simulation proceeds by: (i) defining a regular 10 km grid covering the bounding box of the observation locations (with a 100 km buffer); (ii) generating an unconditional realization of the random field on this grid using `gstat`; (iii) extracting values at the observation locations; and (iv) standardizing to zero mean and unit variance. The range parameter θ_2 is varied to produce random fields with increasing spatial autocorrelation. A disadvantage of this simulation methodology is that the range cannot be steered with precision and there is substantial variation across draws with the same input values. However, the resulting random fields cover the entire spectrum well and the method is thus well suited for the Monte Carlo evaluation. The distribution of observations and the shape of the spatial random fields are illustrated in Figure 5 below.

11.4 Spatial Samples and Random Fields

Figure 5 illustrates the four spatial point samples used throughout the study, each overlaid on a realization of a spatially correlated random field with increasing range parameters. The coarsest lattice (panel a) has large and equal spacing between points, while the finest lattice (panel c) has little spacing. The county centroids (panel d) exhibit highly unequal spacing, with dense coverage in the eastern United States and sparser coverage in the west. As the range parameter increases from 30 km to 90 km, the spatial fields become visibly smoother, reflecting the growing extent of spatial dependence.

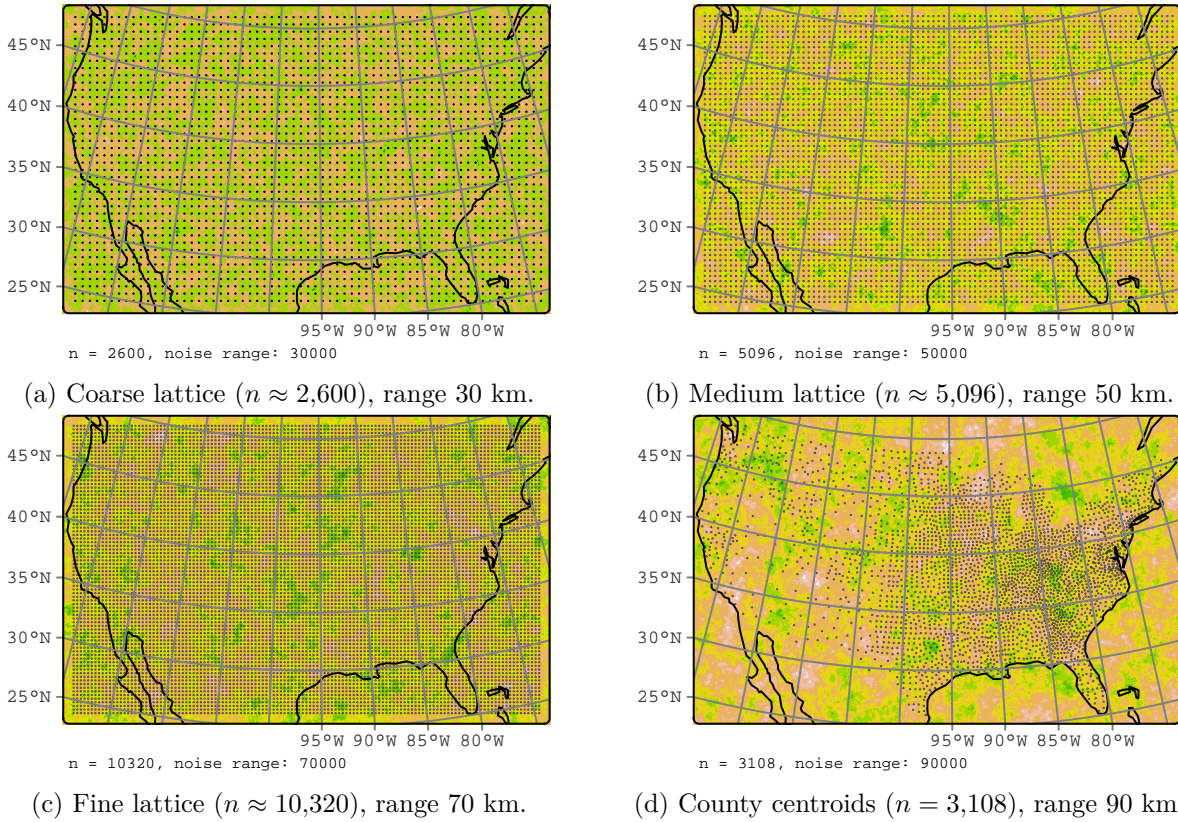


Figure 5: All four spatial point samples overlaid on randomly generated spatial fields with increasing correlation ranges. In the Monte Carlo experiments, each point is assigned the underlying value of the spatial field at its location.

11.5 Handling Non-Stationarity

The covariogram range method relies on the assumption that the spatial correlation structure is stationary (Assumption 1). In practice, many spatial variables exhibit spatial trends—a form of non-stationarity. Common examples include variables that vary systematically with latitude (e.g., temperature-related outcomes) or that cluster around geographic features (e.g., economic activity near coasts or rivers).

Non-stationarity can be addressed within the proposed framework by detrending before applying the covariogram method. The simplest approach is to include location coordinates as control variables in the regression:

$$y_i = \mathbf{x}_i' \beta + f(\text{lon}_i, \text{lat}_i) + \varepsilon_i,$$

where $f(\cdot)$ is a flexible function of geographic coordinates (e.g., a polynomial in longitude and latitude). The covariogram is then computed on the residuals from this augmented regression, which removes the spatial trend and produces a residual process that is closer to stationary.

The Monte Carlo experiments in Section 7 include specifications without longitude and latitude controls. The covariogram-range method performs well in both cases, though including location controls can improve size control when the dependent variable exhibits strong spatial trends.

For variables with extreme non-stationarity—such as distance to a fixed geographic point—the covariogram range method should be applied to residuals from a detrended regression. In such cases, the false positive rate after detrending is substantially reduced compared to the raw regression.